Porous Organic Polymers as Fire-Resistant Additives and Precursors for Hyperporous Carbon towards Oxygen Reduction Reactions

Qingxia Xue[+],[a] Wenjing Li[+],[a] Jinli Dou[+],[a, b] Weiiguo Song,[a] Jingjing Ming,[a] Weiwei Bian,[a] Yuejuan Guo,[a] Xinjian Li,*[a] Weifen Zhang,*[a, b] and Baolong Zhou*[a, b]

Cyclotriphosphazene (CP) based porous organic polymers (POPs) have been designed and prepared. The introduction of CP into the porous skeleton endowed special thermal stability and outstanding flame retardancy to prepared polymers. The nonflammable level of PNK-CMP fabricated via the condensation of 2,2′-(1,4-phenylene)diacetonitrile (DAN) and hexakis(4-acetylphenoxy)cyclotriphosphazene (HACTP) through Knoevenagel reaction, in vertical burning tests reached V-2 class (UL-94) and the limiting oxygen index (LOI) reached 20.8%. When used as additive, PNK-CMP could suppress the dissolving out of PEPA effectively, reducing environment pollution and improving the flame retardant efficiency. The POP and PEPA co-added PU (m_{POP}%: m_{PEPA}% = 5.0%: 5.0%) could not be ignited under simulated real-scale fire conditions. The nonflammable level of POP/PEPA/PU in vertical burning tests (UL-94) reached V-0 class with a LOI as high as 23.2%. The smoke emission could also be suppressed, thus reducing the potential for flame spread and fire hazards. Furthermore, carbonization of PNK-CMP under the activation of KOH yield a hyperporous carbon (PNKA-800) with ultrahigh BET surface area (3001 $m^2 g^{-1}$) and ultramicropore size showing excellent ORR activity in alkaline conditions.

1. Introduction

Porous organic polymers are a burgeoning family of sustainable materials utilizing natural, abundant and renewable precursors. These materials have gained increased attention in recent years.[1] Different to other porous materials, POPs are constructed by pure organic units via covalent bond through various synthetic methods and reactions. These inherent features, such as simple synthetic routes, well-controlled porosity, pre-designable structure and functionality make POPs applicable to various fields, including gas uptake and separation, energy and environment, organic photovoltaic, catalytic and other important areas.[2]

In many cases, the combination of functional monomers and porous properties endowed outstanding performance to the targeted POPs excelling the pure monomers and overcoming the drawbacks existed in the monomers.[3] Inspired by these results, we anticipated to achieve a series of fire-resistant POPs via the introduction of a flame retardant monomer (cyclotriphosphazene). By changing the starting composition of building units and reaction types, two novel CP-based POPs (conjugated PNK-CMP and PNS-CMP) were prepared. Compared with PNS-CMP, PNK-CMP exhibits higher thermal stability and used as the additive or co-additive to the commercial materials studying the flame retardancy performance. Furthermore, the multiple heteroatoms doping structure make these materials ideal precursors for the preparation of porous carbons with controllable element composition which are the most popular materials applied in the renewable energy and environmental related fields, e.g. rechargeable batteries, metal-air batteries,[2] supercapacitors[4] (SCs) and many other new technologies.[5]

2. Results and Discussion

As depicted in Figure 1, PNS-CMP and PNK-CMP were prepared according to the previous reported protocols. Briefly, PNS-CMP was fabricated via the self-polymerization of hexaphenoxycyclotriphosphazene (HPCTP) according to Scholl reaction under the catalytic of $AlCl_3$ in chloroform.[14] PNK-CMP is synthesized via the copolymerization of 2,2′-(1,4-phenylene)diacetonitrile (DAN) and HACTP referred to Knoevenagel reaction under the catalytic of sodium methylate in methyl alcohol/THF mixtures.[15] The detailed procedures are given in the electronic supporting information (ESI). The targeted porous carbons denoted as PNSA-800 and PNKA-

[a] Q. Xue,[+] W. Li,[+] J. Dou,[+] Prof. W. Song, Dr. J. Ming, Prof. W. Bian, Y. Guo, Dr. X. Li, Prof. W. Zhang, Dr. B. Zhou
School of pharmacy, Weifang Medical University, Weifang, 261053, Shandong, P. R. China
E-mail: xinjian89@126.com
zhoubaolong@wfmc.edu.cn
[b] J. Dou,[+] Prof. W. Zhang, Dr. B. Zhou
Shandong Engineering Research Center for Smart Materials and Regenerative Medicine, Weifang Medical University, Weifang, 261053, Shandong, P. R. China
E-mail: zhangwf@wfmc.edu.cn
[+] These authors have equally contributed to this work.

Supporting information for this article is available on the WWW under https://doi.org/10.1002/open.202000059

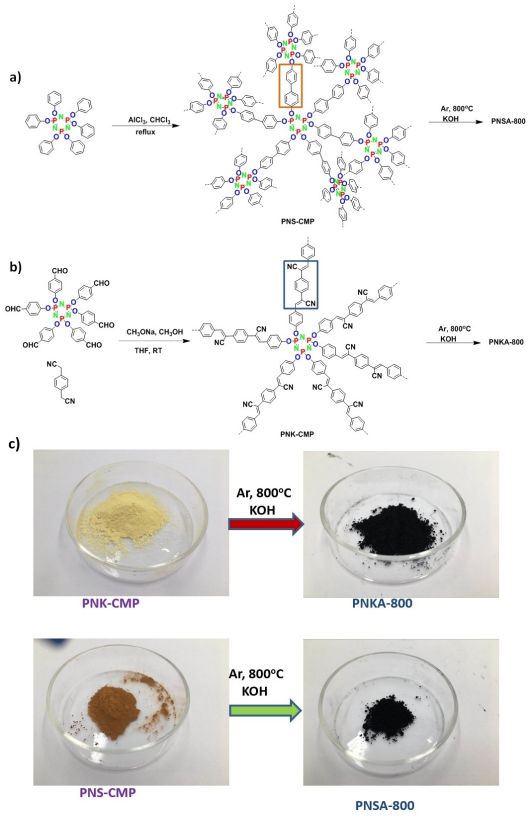

Figure 1. a, b) Route for the preparation of cyclotriphosphazene-based CMPs and corresponding hyperporous carbons with the activation of KOH; c) Schematic of prepared conjugated porous polymers and the resulting porous carbon with the activation of KOH.

800 were fabricated via simple carbonization of prepared CMPs at 800 °C under the activation of KOH in a mass ratio of $M_{polymer}:M_{KOH}=1:2$.[16] The control samples, *i.e.*, PNS-800 and PNK-800 were prepared under the identical conditions but without the activation of KOH. And the detail was given the electronic supporting information.

Figure S1 exhibits the Fourier transform infrared (FT-IR) spectroscopy of prepared samples. Characteristic vibrations bands located at 1220 and 1420 cm^{-1} belonging to the CP ring could be clearly observed for both polymers.[17] Furthermore, feature peaks ascribed to the stretching vibration of newly formed C=C bonds (1596 cm^{-1}) and the inherent C≡N bonds (2218 cm^{-1}) could also be detected from the FTIR of the PNK-CMP.[18] And most important of all, the stretch vibration bands attributed to the carbonyl group around 1690 cm^{-1} is almost disappeared,[19] further validating the successful built-up of the porous skeletons. Figure S2a presents the solid state ^{13}C NMR of as-synthesized polymers, from which strong carbon signals attributed to the phenyl units distributed from 70 to 145 ppm could be found for both polymers. Meanwhile, characteristic peaks of cyano group appeared at 117.3 ppm could be observed from the ^{13}C NMR of CPK-CMP.[18] The solid-state ^{31}P NMR spectroscopy of PNK-CMP were shown in the Figure S2b,[15] typical signals ranged from 0 to 25 ppm assigned to the CP ring could be detected.[20] The corresponding elemental analysis evidenced the coexistence of N, O, C and H for both prepared polymers.

Low temperature N_2 uptake measurements were performed to evaluate the porous properties of prepared materials. As shown in Figure 2a, almost vertical uptake could be observed in the low-pressure region ($P/P_0<0.01$), indicating the existence of micropore for all these prepared materials.[21] With the increasing of pressure, continue increase could be found for all these materials again. However, except the activated samples, obvious hysteresis loop in the medium pressure range and fast-adsorption in the pressure beyond 0.95 could be clearly detected, suggesting significant mesoporosity and the widely existence of macropore for other materials.[22] Meanwhile, the calculated BET surface area for PNK-CMP was only 138 m^2g^{-1}, but it increased to 513 and 3001 m^2g^{-1} for PNK-800 and PNKA-800, respectively. Similar to PNK-CMP, the BET surface areas of PNS-CMP were changed from 173 m^2g^{-1} to 479 (PNS-800) and 1812 m^2g^{-1} (PNSA-800). Besides, both the micro and meso pore volume was also increased, demonstrating large amount of smaller pores were generated during carbonization. All these demonstrate the activation of KOH could further improve the pore properties of POPs, significantly enhancing the surface areas. And that strategy is transferable across other POPs, especially the cyano containing materials to minimize the pronounced swelling effect in the porous adsorbed species. Figure 2b presents the pore size distributions curves of prepared samples. PNK-CMP shows a main peak at 2.18 nm with secondary peaks at 1.60, 2.74 and 3.79 nm, respectively. PNS-CMP exhibits a main peak at 2.10 nm with small peaks at 1.34, 2.48 and 3.89 nm, respectively, indicating hierarchical pore structure for prepared polymers. However, the pore size is centered at micropore ranges for the carbonized samples, e.g., PNKA-800 are located at 0.57 nm and PNSA-800 are situated at 1.43 nm, implying the substantially increased micropore.[4] And the detail about the porosity was listed in Table S1.

Field emission scanning electron microscope (FE-SEM) and TEM were performed to investigate the microstructure of as-synthesized samples. Figure 3a and Figure 3d showed the SEM of prepared polymers, from which, bulk stacked by aggregated spherical nanoparticles could be observed for both polymers. As presented in Figure 3g, 3j and Figure S3, the morphology could be maintained at a great extent after

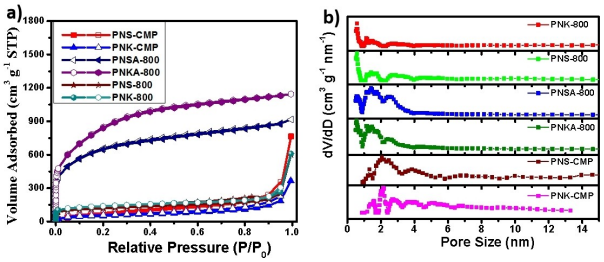

Figure 2. a) Nitrogen adsorption and desorption isotherm of prepared materials at 77 K; b) Pore-width distribution curves of prepared materials.

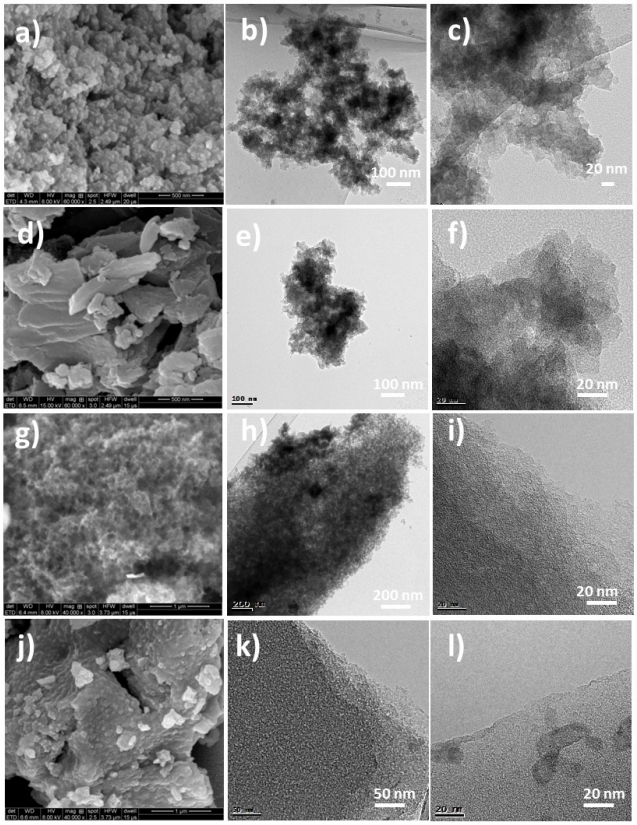

Figure 3. SEM and TEM of prepared polymers and corresponding porous carbon. a) SEM of PNS-CMP; b, c) TEM of PNS-CMP in scale bar of 100 and 20 nm, respectively; d) SEM of PNK-CMP; e, f) TEM of PNS-CMP in scale bar of 100 and 20 nm, respectively; g) SEM of PNSA-800; h, i) TEM of PNKA-800 in the scale bar of 50 and 20 nm, respectively; j) SEM of PNSA-800; k, l) TEM of PNSA-800 in scale bar of 50 and 20 nm, respectively.

the activation. Widely distributed pore, ascribed to the inherent skeleton structure or the space generated by the pile up of particles, could be detected from the TEM given in Figure 3b–c, 3e–f, 3h–i, 3k–l, and Figure S3 by the light and shade contrast.

Like in previous report, the powder XRD patterns validate amorphous structure of prepared polymers (Figure S4a). And still, no clear peaks could be observed from the XRD of annealing samples (Figure S4b), indicative the amorphous features of prepared porous carbon. TGA were performed to examine the thermal stability of prepared polymers. According to Figure S5, owing to the high polarity of prepared polymers, dramatically weight loss attributed to the evaporation and desorption of adsorbed water (16.3% for PNK-CMP and 6.8% for PNS-CMP) could be observed at the low temperature range. Even at the temperature of 800 °C, the remaining carbon is beyond 55 wt% for PNK-CMP (vs 32% of PNS-CMP), suggesting the super thermal stability of CP-based CMPs. Raman spectra of pyrolysis samples all displayed two intensive peaks around 1347 and 1586 cm^{-1}, assigned to the D band and G band, respectively (Figure S6).[23] All these samples present high graphitic degree with a high intensity ratio of G band to D band (I_D/I_G). For example, the intensity ratio of PNKA-800 is 0.98, and it reaches 0.95 for PNSA-800.

Figure 4 and Figure S7 displayed the X-ray photoelectron spectroscopy (XPS) of PNKA-800 and PNSA-800, respectively. The XPS survey spectrum of PNKA-800 (Figure 4a), shows obvious signals belonging to the C, N, O, and P, validating the existence of afore mentioned element in prepared carbon samples. Figure 4b shows the high-resolution C1s spectra, a dominant peak at 284.8 eV, combined with two small peaks distributed at 285.9 eV and 287.6 eV could be observed.[24] As presented in the Figure 4c, the N 1s spectra could be deconvoluted into three peaks located at 398.8, 399.8, and 401.1 eV, corresponding to the pyridine, pyrrole, and graphitic N species, respectively.[25] High resolution P 2p peaks could be divided into two peaks, situated at 133.2 and 133.9 eV (Figure 4e), attributing to P–C bond and P–O bond, respectively.[26] In accordance with the previous results, two obvious peaks at 530.9 and 532.4 eV, assignable to the C–O and C–P bond, could be obviously observed.

The special features of PNKA-800, especially the ample N, P content, stimulate us to study electrocatalytic property towards oxygen reduction in alkaline conditions (O_2-saturated 0.1 M KOH solution). Figure 5a presents the LSV curves of PNKA-800 and Pt/C at 1600 rpm. PNKA-800 shows a onset potential (E_{onset}) of 0.935 V as well as a half-wave potential ($E_{1/2}$) of 0.756 V, 75 and 27 mV negative than the commercial Pt/C, but comparable or even positive than these of other reported P and N co-doped carbon materials and the detailed comparisons towards the ORR activities is listed in Table S2.

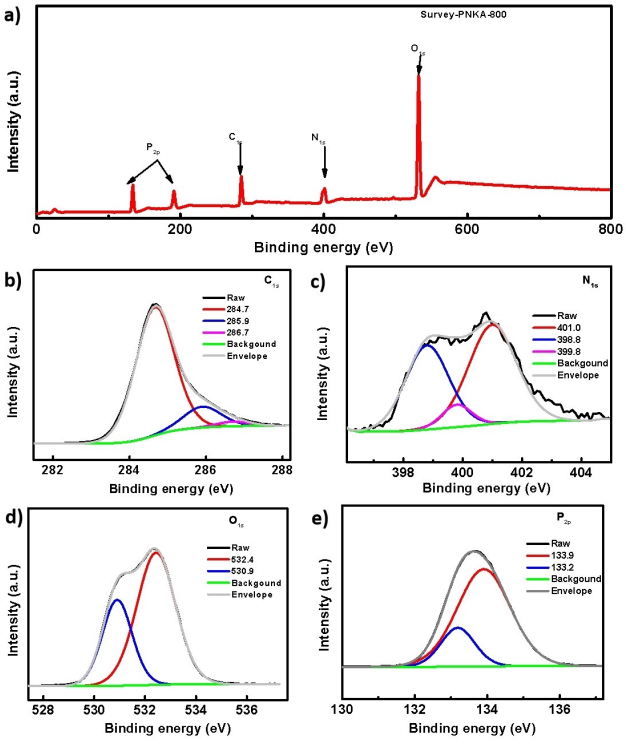

Figure 4. XPS of PNKA-800. a) Survey spectrum of PNKA-800; b) High-resolution XPS C 1s of PNKA-800; c) N 1s spectrum of PNKA-800; d) High-resolution XPS O 1s of PNKA-800; e) P 2p spectrum of PNKA-800.

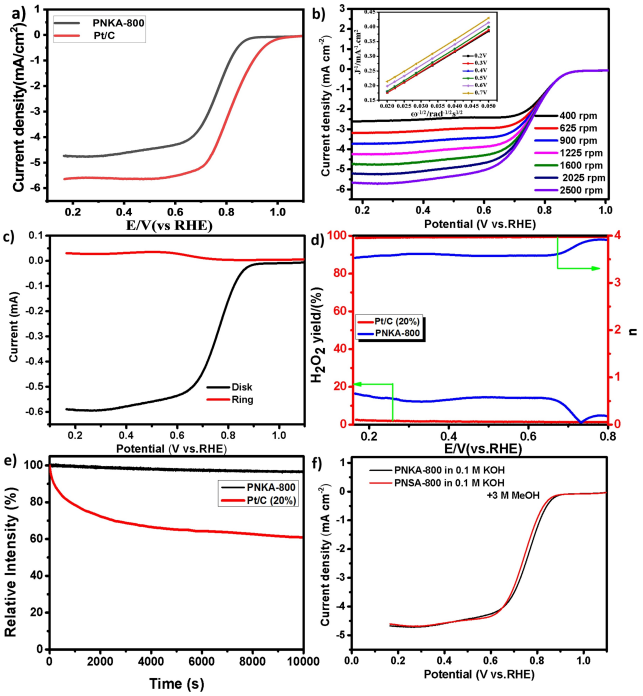

Figure 5. Electrocatalytic performance of PNKA-800 for ORR in O_2-saturated 0.1 M KOH. a) Current potential characteristics of PNKA-800 and 20 wt% Pt/C at a scan rate of 5 mV s^{-1} with rotation speed of 1600 rpm; b) Polarization curves of PNKA-800 with a sweep rate of 5 mV s^{-1} at different rotation rates and the insert part is the K–L plots of PNKA-800 at different potentials; c) Ring and disk current measured from the Rotating ring-disk electrode (RRDE) scanned at 5 mV s^{-1} at 1600 rpm, the Pt ring was polarized at 1.5 V (vs. RHE) in alkaline electrolyte; d) The H_2O_2 yield and electron transfer number (n) curves obtained from the RRDE measurements; e) Durability evaluation from chronoamperometric responses; f) Polarization curves measured before and after the methanol-crossover test with a scan rate of 5 mV s^{-1}.

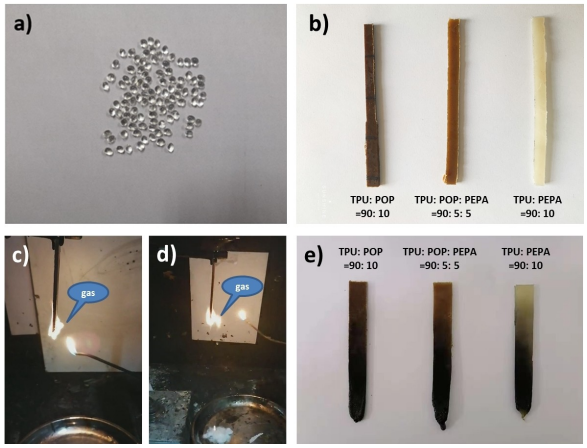

Figure 6. Digital photograph of pure or prepared TPU composites. a) Digital photograph of pure TPU; b) Digital photograph of TPU/POP/PEPA composites in different mass ratio (90:10:0), TPU/POP/PEPA composites in a mass ratio of 90:5:5 and TPU/POP/PEPA composites in a mass ratio of 90:0:10 c) and d) Digital photograph of the flame released during combustion of POP/TPU composites; e) Digital photograph of POP/PEPA/TPU composites after the vertical burning tests.

Furthermore, PNKA-800 exhibits a limited current density of 4.75 mA cm^{-2} at 0.2 V (vs. 5.51 mA cm^{-2} at 0.2 V). Figure S6 displayed the CV curves of PNKA-800. In contrast to the featureless curve in Ar-saturated solution, obvious cathodic peak could be clearly detected in the O_2 saturated solution. Figure 6b exhibited the polarization curves of PNKA-800 measured from 400 rpm to 2500 rpm, and the insert part is the corresponding Koutecky-Levich (K–L) plots calculated according the Equation S1. The electron-transfer number (n) obtained from the slopes of K–L plots are 3.75 at the potential of 0.2 V, suggesting a four-electron pathway for ORR. And that could also be validated by the RRDE measurements shown in in Figure 5c and 5d. The calculated electron transfer number according to the Equation S3 and S4 are ranged from 3.51 to 3.96, close to that of the commercial Pt/C with a low H_2O_2 yield below 17.1% in the region from 0.2 to 0.8 V and consistent well with the result obtained from the K–L plots, further determining a high selectivity towards the four-electron reduction pathway of oxygen. For the real application of as-synthesized sample, an excellent cycle stability is desired. Hence, i-t test was conducted at static potential of 0.6 V (vs. RHE). Figure 5e presented the time dependent current density curves of PNKA-800. After a continuous running of 20000 s, only a negligible loss of 3.1% of the initial current was detected for the synthesized sample, much better than that of commercial Pt/C catalyst (37.2%), indicative PNKA-800 possessing superior durability. Figure 5f shows the polarization curves measured before and after the methanol-crossover test, almost identical curves were found with a negative shift of 10 mV in $E_{1/2}$ (vs 37 mV for Pt/C given in Figure S8). All these results evidenced PNKA-800 can act as a remarkable oxygen reduction electrocatalyst in alkaline solution applied in the metal-air battery.

For the unique structure, cyclotriphosphazene (CP) and CP-derived materials are widely investigated as the flame retardant additive, lowering smoke emission and heat release rate. Pentaerythritol octahydrogen tetraphosphate (PEPA) is a commercial flame retardant commonly used as additive in thermoplastic polyurethane elastomer (TPU), improving the flame retardant efficiency. A minimum addition of 10% can play a better flame retardant effect. But PEPA could migrate out from the TPU which are harmful to the environment.

The similarity of structure and elemental composition for the PEPA and POP, make PEPA easily get into the hole of PNK-CMP. Inspired by this, we anticipated to inhibit the releasing of PEPA from the TTU via introduction of porous CMP. It is the first time that the porous PNK-CMP was applied as additive or co-additive with PEPA to commercially available TPU improving the flame retardant efficiency. As shown in Figure 6, CMP/TPU was fabricated via simple physical processing in different mass ratios of POP to TPU. One could observe clearly that the color of composites darkens with the increasing of mass ratio. While, CMP/PEPA/TPU composites was prepared stepwise. PEPA was initially absorbed in the porous skeleton of CMP, then the composites was mixed with the TPU (mPOP%:mPEPA% = 5.0%:5.0%).

To evaluate the flammability, vertical burning tests (UL-94) and limiting oxygen index (LOI) measurements were

conducted. In UL-94 tests, the TPU/POP/PEPA composites possessed the highest level (V-0), similar to the TPU/PEPA, but higher than that of TPU/CMP composites (V-2). As shown in Table 1 and Video S1, S2, even directly exposed to an igniter for 10 s, the TPU/POP/PEPA sample could not be ignited. When the igniter was removed, the flame was extinguished instantly, and no obvious flame was observed on the surface of samples. After that test, compared with the TPU/POP composites, TPU/POP/PEPA maintained the original shape better, suggesting certain flame retardancy. Furthermore, as delivered in Figure 5c and 5d, large amount of nonflammable gas (N_2) was generated during the combustion process, released by the decomposition of composites, which are further transformed into protective carbon-layer coated on the material surface (Figure 5e). Meanwhile, the lOI value reaches 25.2% for the TPU/POP/PEPA composites higher than the TPU/POP composites (23.0%). The POP and PEPA co-added TPU ($m_{POP}\%:m_{PEPA}\%:m_{TPU}\% = 5.0\%:5.0\%:90\%$) could not be ignited under simulated real-scale fire conditions. And as observed form Figure 5c, 5d and 5e, a large amount of nonflammable gas was emitted from materials preventing the burning, after combustion carbon-layer was formed which to prevent further transfer heat to composites. This process conforms to the mechanism of intumescent flame retardant. Furthermore, when used as additive, PNK-CMP could suppress the dissolving out of commercial PEPA effectively, reducing environment pollution and improving the flame retardant efficiency. In contrast, TPU polymer insulation materials are easily ignited. Furthermore, the fire retardancy could also be validated by the TGA given in the Figure S9. Compared with the pure polymer, the thermal stability of composites enhanced greatly. And the ternary complex ($m_{POP}\%:m_{PEPA}\%:m_{TPU}\% = 5.0\%:5.0\%:90\%$) presents a TG similar to the binary complex ($m_{PEPA}\%:m_{TPU}\% = 10\%:90\%$).

3. Conclusions

In summary, cyclotriphosphazene based CMPs were well-designed and facilely prepared. The special elemental composition and special thermal stability endowed these polymers ideal candidates for multiple atoms doped porous carbon applicable for the energy and environment-related fields. Under the activation of KOH, hyperporous carbon with ultrahigh BET surface area of 3001 $m^2 g^{-1}$ and ultra uniform pore size distribution were obtained which could further be used as the carbon-based catalysts for ORR with excellent performance. The introduction of CP into the porous skeletons give outstanding flame retardancy to prepared polymers. And the porous features could suppress the dissolving out of commercial PEPA effectively, reducing the pollution triggered by traditional flame retardant. For example, the nonflammable level of POP and PEPA co-added TPU ($m_{POP}\%:m_{PEPA}\% = 5.0\%:5.0\%$) reached V-0 class with a LOI as high as 23.2% that could not be ignited under simulated real-scale fire conditions.

Table 1. Formulations and Flame retardant data of TPU composites.

samples	ratio	LOI [%]	UL-94 t1/t2[s]	Cotton ignition	rating
Pure TPU	–	20.2±0.3	–/–	Yes	NR
TPU/POP	90:10	23.0±0.2	5/0	Yes	V-2
TPU/POP/PEPA	90:5:5	25.2±0.2	2/0	No	V-0
TPU/PEPA	90:10	27.0±0.2	0/0	No	V-0

Acknowledgments

This work was supported by the National Natural Science Foundation of China (81774125 and 81973671).

Conflict of Interest

The authors declare no conflict of interest.

Keywords: cyclotriphosphazene · porous organic polymers · fire-resistant additive · hyperporous carbons · ORR

[1] B. Zhou, F. Yan, X. Li, J. Zhou, W. Zhang, *ChemSusChem* **2019**, *12*, 915.
[2] a) A. D. Roberts, X. Li, H. Zhang, *Chem. Soc. Rev.* **2014**, *43*, 4341; b) Z. Xu, L. Hu, J. Ming, X. Cui, M. Zhang, J. Dou, W. Zhang, B. Zhou, *Microporous Mesoporous Mater.* **2020**, DOI: org/10.1016/j.micromeso.2020.110259.
[3] a) M. Titirici, R. White, N. Brun, V. L. Budarinet, D. Su, F. Monte, J. H. Clarkd, M. J. MacLachlang, *Chem. Soc. Rev.* **2015**, *44*, 250; b) M. Zhang, J. Ming, W. Zhang, J. Xie, P. Lin, X. Song, X. Chen, X. Wang, B. Zhou, *ACS Omega* **2020**, *5*, 7225.
[4] a) B. Zhou, L. Liu, P. Cai, G. Zeng, X. Li, Z. Wen, L. Chen, *J. Mater. Chem. A* **2017**, *5*, 22163; b) M. Zhang, T. Zhao, J. Dou, Z. Xu, W. Zhang, X. Chen, X. Wang, B. Zhou, *ChemElectroChem* **2019**, *6*, 5946.
[5] a) G. Zeng, X. Hu, B. L. Zhou, J. X. Chen, C. S. Cao, Z. H. Wen, *Nanoscale* **2017**, *9*, 14722; b) Y. Wang, Y. Song, Y. Xia, *Chem. Soc. Rev.* **2016**, *45*, 5925; c) Q. Xue, Z. Xu, D. Jia, X. Li, M. Zhang, J. Bai, W. Li, W. Zhang, B. Zhou, *ChemElectroChem* **2019**, *6*, 4491; d) Q. Pan, Z. Xu, S. Deng, F. Zhang, H. Li, Y. Cheng, L. Wei, J. Wang, B. Zhou, *RSC Adv.* **2019**, *9*, 39332.
[6] a) X. Yang, L. Chen, Y. Li, J. C. Rooke, C. Sanchez, B. Su, *Chem. Soc. Rev.* **2017**, *46*, 481; b) V. D. Netha, S. Rana, H. J. Yoo, A. Chaurasia, J. McLeskey, J. T. Ramasamy, M. S. Ramasamyc, N. G. Sahoo, J. W. Cho, W. Cho, *Prog. Polym. Sci.* **2017**, *67*, 1.
[7] A. H. Lu, F. Schuth, *Adv. Mater.* **2006**, *18*, 1793.
[8] E. Frackowiak, *Phys. Chem. Chem. Phys.* **2007**, *9*, 1774.
[9] Y. Xu, S. Jin, H. Xu, A. Nagai, D. Jiang, *Chem. Soc. Rev.* **2013**, *42*, 8012.
[10] A. I. Cooper, *Adv. Mater.* **2009**, *21*, 1291.
[11] H. G. Wang, Z. H. Cheng, Y. Z. Liao, J. H. Li, J. Weber, A. Thomas, C. F. J. Faul, *Chem. Mater.* **2017**, *29*, 4885.
[12] M. Salanne, B. Rotenberg, K. Naoi, K. Kaneko, P. L. Taberna, C. P. Grey, B. Dunn, P. Simon, *Nat. Energy.* **2016**, *1*, 16070.
[13] B. Li, M. Zheng, H. Xue, H. Pang, *Inorg. Chem. Front.* **2016**, *3*, 175.
[14] a) S. Meng, H. P. Ma, L. C. Jiang, H. Ren, G. S. Zhu, *J. Mater. Chem. A* **2014**, *2*, 14536; b) B. Y. Li, Z. H. Guan, X. J. Yang, W. D. Wang, W. Wang, I. Hussain, K. P. Song, B. Tan, T. Li, *J. Mater. Chem. A* **2014**, *2*, 11930.
[15] Y. B. Wei, W. B. Chen, X. Y. Zhao, S. Y. Ding, S. Han, L. Chen, *Polym. Chem.* **2016**, *7*, 3983.
[16] a) J. S. M. Lee, M. E. Briggs, T. Hasell, A. I. Cooper, *Adv. Mater.* **2016**, *28*, 9804; b) S. I. Gu, J. Q. He, Y. L. Zhu, Z. Q. Wang, D. Y. Chen, G. P. Yu, C. Y. Pan, J. G. Guan, K. Tao, *ACS Appl. Mater. Interfaces* **2016**, *8*, 18383.
[17] a) J. S. M. Lee, M. E. Briggs, T. Hasell, A. I. Cooper, *Adv. Mater.* **2016**, *28*, 9804; b) S. Gu, J. Q. He, Y. Zhu, Z. Wang, D. Chen, G. Yu, C. Pan, J. Guan, K. Tao, *ACS Appl. Mater. Interfaces* **2016**, *8*, 183.
[18] X. D. Zhuang, W. X. Zhao, F. Zhang, Y. Cao, F. Liu, S. Bia X. L Feng, *Polym. Chem.* **2016**, *7*, 4176.

[19] E. Q. Jin, M. Z. Asada, Q. Xu, S. Dalapati, M. A. Addicoat, M. A. Brady, H. Xu, T. Nakamura, T. Heine, Q. H. Chen, D. L. Jiang, *Science* **2017**, *357*, 673.
[20] P. Mohanty, L. D. Kull, K. Landskron, *Nat. Commun.* **2011**, *2*, 401.
[21] B. Zhou, X. Hu, G. Zeng, S. W. Li, Z. Wen, L. Chen, *ChemSusChem* **2017**, *10*, 2955.
[22] S. L. Candelaria, B. B. Garcia, D. Liu, G. Cao, *J. Mater. Chem.* **2012**, *22*, 9884.
[23] Z. Zhao, S. Hao, P. Hao, Y. Sang, A. Manivannan, N. Wu, H. Liu, *J. Mater. Chem. A* **2015**, *3*, 15049.
[24] Z. Zhang, J. Sun, F. Wang, L. Dai, *Angew. Chem. Int. Ed.* **2018**, *130*, 9176.
[25] X. Zhu, T. Jin, C. Tian, C. Lu, X. Liu, M. Zeng, X. Zhuang, S. Yang, L. He, H. Liu, S. Dai, *Adv. Mater.* **2017**, *2*, 1704091.
[26] a) J. Zhang, L. Qu, G. Shi, J. Liu, J. Chen, L. Dai, *Angew. Chem. Int. Ed.* **2016**, *128*, 2270; b) W. Wan, Q. Wang, L. Zhang, H. Liang, P. Chen, S. Yu, *J. Mater. Chem. A* **2016**, *4*, 8602.

Manuscript received: March 3, 2020
Revised manuscript received: April 24, 2020